Metal-insulator transition in a weakly interacting disordered electron system

C. E. Ekuma, S.-X. Yang, H. Terletska, K.-M. Tam, N. S. Vidhyadhiraja, J. Moreno, and M. Jarrell

Phys. Rev. B **92**, 201114 — Published 25 November 2015

DOI: 10.1103/PhysRevB.92.201114

Metal-Insulator-Transition in a Weakly interacting Disordered Electron System

C. E. Ekuma,[1,2,*] S.-X. Yang,[1,2] H. Terletska,[1,2] K.-M. Tam,[1,2] N. S. Vidhyadhiraja,[3] J. Moreno,[1,2] and M. Jarrell[1,2,†]

[1] *Department of Physics & Astronomy, Louisiana State University, Baton Rouge, Louisiana 70803, USA*
[2] *Center for Computation and Technology, Louisiana State University, Baton Rouge, Louisiana 70803, USA*
[3] *Theoretical Sciences Unit, Jawaharlal Nehru Center for Advanced Scientific Research, Bangalore, 560064, India*

The interplay of interactions and disorder is studied using the Anderson-Hubbard model within the typical medium dynamical cluster approximation. Treating the interacting, non-local cluster self-energy ($\Sigma_c[\tilde{\mathcal{G}}](i, j \neq i)$) up to second order in the perturbation expansion of interactions, U^2, with a systematic incorporation of non-local spatial correlations and diagonal disorder, we explore the initial effects of electron interactions (U) in three dimensions. We find that the critical disorder strength (W_c^U), required to localize all states, increases with increasing U; implying that the metallic phase is stabilized by interactions. Using our results, we predict a soft pseudogap at the intermediate W close to W_c^U and demonstrate that the mobility edge (ω_ϵ) is preserved as long as the chemical potential, μ, is at or beyond the mobility edge energy.

PACS numbers: 72.15.Rn,02.70.Uu,64.70.Tg,71.23.An,71.27.+a

Introduction.– The metal-insulator transition (MIT) driven by random impurity has been an important topic in physics since the pioneer work by Anderson [1]. A significant advance in the MIT theory is achieved by studying it in the context of critical phenomena. Concepts from scaling, renormalization group (RG), and random matrix theory are used to understand the mechanism of localization at different dimensions for different symmetry classes [2–5]. It has been demonstrated that an infinitesimal amount of disorder can lead to localization for the models in the orthogonal class at lower (one and two) dimensions, whereas there is a MIT for three dimensions (3D) [2]. In 3D, a sharp mobility edge separating localized and delocalized states develop as disorder strength increases [6].

While the MIT of non-interacting systems by now is fairly well understood [4, 5, 7], earlier studies suggested that interaction could play an important role in the MIT [8]. Over the last few decades, experimental works ranging from doped semiconductors [6, 9, 10], perovskite compounds [11–15]), to cold atoms in optical lattices[16–19] have highlighted the importance of the interplay of disorder (W) [1, 2, 4, 5] and interactions (U) [6].

At the Fermi level, Altshuler-Aronov [20] showed that interactions can induce a square-root and logarithmic singularity in two and three dimensions, respectively, while Efros-Shklovskii demonstrated the Coulomb gap [21]. Field theory perturbative RG method and diagrammatic theory which go beyond the Hartree-Fock approximations have suggested a metallic state for two dimensions [22, 23]. The recent RG work by Finkelstein and co-workers has further indicated the possibility of a MIT for a model with degenerate valleys [24], the validity of which was confirmed through experiments in Si-MOSFETs [24, 25].

In this letter, we focus on the system with weak local interactions on disorder systems in 3D. Our approach is an extension of the recently developed typical medium dynamical cluster approximation (TMDCA), which has shown to be highly successful in describing the Anderson localization transition (ALT) for the non-interacting systems [26]. The typical medium approaches assume that the typical density of states (TDoS), when appropriately defined, acts as the "proper" order parameter for the ALT. Such an assumption is well justified not only for the non-interacting case [26–28] but also in the presence of interactions, as shown experimentally[9, 29]. The typical medium theory (TMT) of Dobrosavljević *et al* [27] is a special case of the TMDCA when the cluster size $N_c = 1$. Even though the TMT cannot include weak localization effects due to coherent backscattering, it still does qualitatively predict a disorder-driven ALT, and hence incorporates 'strong localization' effects. The TMDCA incorporates non-local effects via systematic finite cluster increment and achieves almost perfect agreement with numerical exact calculations. The extension of the TMT to finite interactions show that interactions screen the disorder[30–32]. In this letter, we show that such a conclusion is robust in the thermodynamic limit through increasing cluster size calculations.

While there have been significant efforts to understand the combined effect of disorder and interactions on the local density of states close to the Fermi level, the band edges have received scant attention. Specifically, the effect of weak interactions on the mobility edge has not been discussed thus far. We are particularly interested in the evolution of the mobility edge under the influence of the Hubbard interaction for spin$-1/2$ system. The transition between metal–the Fermi liquid phase; and insulator–the Anderson localized phase is discussed, whereas the possibility of the Mott insulator is excluded in this study, as only short range, weak interactions will be considered.

The main result of this letter is that for $\mu < \omega_\epsilon$,

arbitrary small interactions lead to the masking of the sharp mobility edge that separates localized and extended states in the non-interacting regime below the critical disorder strength $W_c^{U=0}$. Thus, interactions can radically modify the spectrum of a non-interacting system at the band edges, i.e., in the 'localized band'. However, when the chemical potential (μ) is at or above the mobility edge energy (i.e., $\mu \geqq \omega_\epsilon$), the well-defined localization edge is restored. Nevertheless, unlike the non-interacting systems where the TDoS just shifts rigidly as one scans through μ, in the presence of interactions, there is a non-trivial decrease of the TDoS vis-à-vis the change in the filling. Further, we find a soft-pseudogap at intermediate W just below W_c^U.

Method.– The Anderson-Hubbard model (AHM) is a model for studying the interplay between electron–electron interactions and disorder. The Hamiltonian for this model is

$$H = -\sum_{\langle ij\rangle\sigma} t_{ij}(c^\dagger_{i\sigma}c_{j\sigma}+h.c.)+\sum_{i\sigma}(V_i-\mu)n_{i\sigma}+U\sum_i n_{i\uparrow}n_{i\downarrow}. \tag{1}$$

The first term describes the hopping of elect rons on the lattice, $c_i^\dagger(c_i)$ is the creation (annihilation) operator of an electron on site i with spin σ, $n_i = c_i^\dagger c_i$ is the number operator, $t_{ij} = t$ is the hopping matrix element between nearest-neighbor sites. The second term represents the disorder part which is modeled by a local potential V_i randomly distributed according to a probability distribution $P(V_i)$, μ is the chemical potential. The last term describes the Coulomb repulsion between two electrons occupying site i. We set $4t = 1$ as the energy unit and use a "box" distribution with $P(V_i) = \frac{1}{2W}\Theta(W - |V_i|)$, where $\Theta(x)$ is the Heaviside step function. We use the short-hand notation: $\langle ...\rangle = \int dV_i P(V_i)(...)$ for disorder averaging.

Our focus is on the single-particle Green function and the associated density of states. To obtain these for the AHM (1), we modify the TMDCA to treat both disorder and interactions. Here, an initial guess for the hybridization function ($\Gamma(\mathbf{K},\omega) \equiv \Im 10^{-2}$) is used to form the cluster-excluded Green function $\mathcal{G}(\mathbf{K},\omega) = (\omega - \Gamma(\mathbf{K},\omega) - \bar{\epsilon}_{\mathbf{K}} + \mu)^{-1}$, where $\bar{\epsilon}_{\mathbf{K}}$ is the coarse-grained bare dispersion. $\mathcal{G}(\mathbf{K},\omega)$ is then Fourier transformed to form the real space Green function, $\mathcal{G}_{n,m} = \sum_{\mathbf{K}} \mathcal{G}(\mathbf{K})\exp(i\mathbf{K}\cdot(\mathbf{R}_n-\mathbf{R}_m))$ and then for a given disorder configuration $\hat{V}$, we may calculate the cluster Green function $G^c(\hat{V}) = (\mathcal{G}^{-1} - \hat{V})^{-1}$.

Utilizing $G^c(\hat{V})$, we then calculate the Hartree-corrected cluster Green function $\tilde{\mathcal{G}}_c^{-1}(\hat{V},U) = G^c(\hat{V})^{-1} + \epsilon_d(U)$ (where $\epsilon_d(U) = \tilde{\mu} - U\tilde{n}_i/2$ and $\tilde{n}_i = -1/\pi\int_{-\infty}^{0}\Im\tilde{\mathcal{G}}_c(i,i,\omega)d\omega$ is the site occupancy at zero temperature, $T = 0$). Both $\tilde{\mathcal{G}}$ and $\tilde{n}_i$ are converged and then used to compute the second-order diagram shown in Fig. 1. We note that $\tilde{n}_i$ obtained at $\tilde{\mathcal{G}}_c$-level is numerically the same as using the full Green function since $\tilde{n}_i$ is self-consistent at the TMDCA level. This also enables the incorporation of crossing diagrams (for $N_c > 1$) from both disorder and interactions at equal footing and it is computationally cheaper (for $N_c = 1$, it is ~ 8 times cheaper), enabling simulation of large systems.

Here, we choose the chemical potential $\tilde{\mu} = \mu + U/2$ to enable simulations both at and away from half-filling. Thus, the full self-energy due to interactions is then $\Sigma_c^{Int}(i,j,\omega) = \Sigma_c^H[\tilde{\mathcal{G}}] + \Sigma_c^{(SOPT)}[\tilde{\mathcal{G}}]$, where the first term is the static Hartree correction and the second term is the non-local second-order perturbation theory (SOPT) contribution. We note that the computational cost grows exponentially with each order of the perturbation series making it numerically prohibitive to include more diagrams. However, since our focus is on the weak interaction regime $U/4t \ll 1$, we expect that higher order diagrams are suppressed by at least $\sim U^3$.

We have carried out extensive benchmarking of the TMDCA-SOPT cluster solver against numerically exact quantum Monte-Carlo calculations [33–41] within the dynamical cluster approximation (DCA) framework. For weak interactions and essentially all disorder strengths, the corrections due to perturbation orders higher than the second are found to be negligible (for details, see Supplemental Material (SM) [42]).

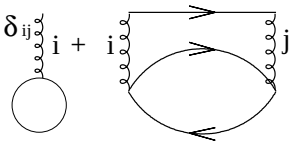

FIG. 1. The first and second-order diagrams of the interacting self-energy between sites i and j.

For a given interaction strength U and randomly chosen disorder configuration V, we calculate the fully dressed cluster Green function $\tilde{G}^c(\hat{V},U) = (\mathcal{G}^{-1} - \hat{V} - \Sigma^{Int}(U) + U/2)^{-1}$. With $\tilde{G}^c(\mathbf{K},\omega,V,U)$, we calculate the typical density of states as

$$\rho^c_{typ}(\mathbf{K},\omega) = \exp\left(\frac{1}{N_c}\sum_{i=1}^{N_c}\langle\ln\rho_i^c(\omega,V)\rangle\right)\left\langle\frac{\rho^c(\mathbf{K},\omega,V)}{\frac{1}{N_c}\sum_i\rho_i^c(\omega,V)}\right\rangle \tag{2}$$

following the prescriptions of Ref. [26], which avoids self-averaging. The disorder and interaction averaged typical cluster Green function is obtained using the Hilbert transform $G^c_{typ}(\mathbf{K},\omega) = \int d\omega'\rho^c_{typ}(\mathbf{K},\omega')/(\omega-\omega')$. We close the self-consistency loop by calculating the coarse-grained cluster Green function of the lattice $\overline{G}(\mathbf{K},\omega) = \int\frac{N_0^c(\mathbf{K},\epsilon)d\epsilon}{(G^c_{typ}(\mathbf{K},\omega))^{-1} + \Gamma(\mathbf{K},\omega) - \epsilon + \overline{\epsilon}(\mathbf{K})}$, where $N_0^c(\mathbf{K},\epsilon)$ is the bare partial density of states.

Results and Discussion– We start the analysis of our results by comparing the algebraic (or average) density of states (ADoS) (obtained from the DCA, where the algebraic averaging is utilized in the self-consistency) and the typical density of states (TDoS) (obtained from the TMDCA-SOPT, where the self-consistency environment is defined by a typical medium) for a finite cluster $N_c = 38$ at various disorder strengths for $U = 0.0$ and 0.1 at

half-filling (Figs. 2(a) and (b)).

At weak disorder, $W \sim 0.5$, the TDoS resembles the ADoS. However, for larger W, comparing the $U = 0.0$ results (Fig. 2(a)) with those of $U = 0.1$ (Fig. 2(b)), a noticeable renormalization of the spectrum is observed. There is a gradual suppression of the TDoS as the disorder strength is increased for both $U = 0.0$ and 0.1. The TDoS at $\omega = 0$ is noticeably larger when the U is finite. This indicates a delocalizing effect of interactions which is consistent with a real space renormalization group study [43] and has been interpreted as a screening of the disorder [30, 44]. For a given disorder strength, the band edges at half-filling for the interacting case appear to be identical to that of the $U = 0$ spectrum. This seems to imply that the mobility edge is preserved when U is turned on. However, this is not the case, and this becomes clear upon examining the tails of the density of states.

To explore the effect of weak interactions on the localization edge of a disordered electron system, we show in Fig. 3, the evolution of the TDoS with $\delta = W/W_c^U$ for various values of U on a linear log plot at various μ. Clearly for $U = 0$, a sharp, well-defined mobility edge is observed (see also Fig.2(a)). However, even for a very small $U = 0.1$ (1/30 of the bandwidth), and for both the TMT and TMDCA-SOPT, the sharp localization edge is replaced by an exponential tail, when $\mu < \omega_\epsilon$. Hence, the incorporation of Coulomb interactions in the presence of disorder for $\mu < \omega_\epsilon$ leads to long band tails that are exponentially decaying. This fingerprint can be understood from a Fermi liquid perspective.

If we inject an electron into a Fermi liquid with an energy ω above the Fermi energy, then, we expect the particle to experience an inelastic scattering, due to U which is proportional to ω^2. One factor of ω is due to energy conservation and the other to momentum conservation with

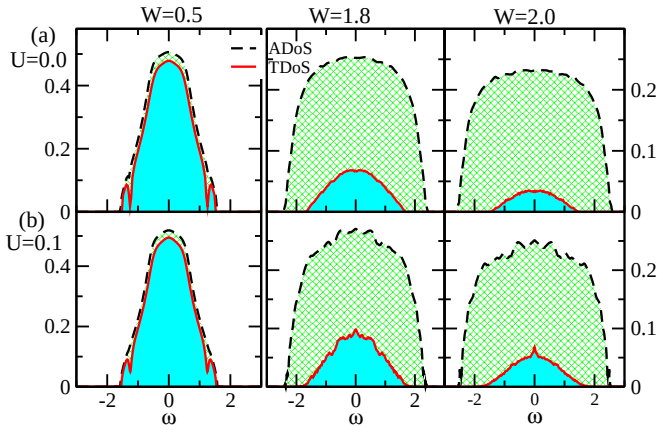

FIG. 2. (Color online). Evolution of the ADoS and TDoS at various W at $U = 0$ (**a**) and $U = 0.1$ (**b**) for the TMDCA-SOPT with $N_c = 38$ for the half-filled Anderson-Hubbard model (AHM).

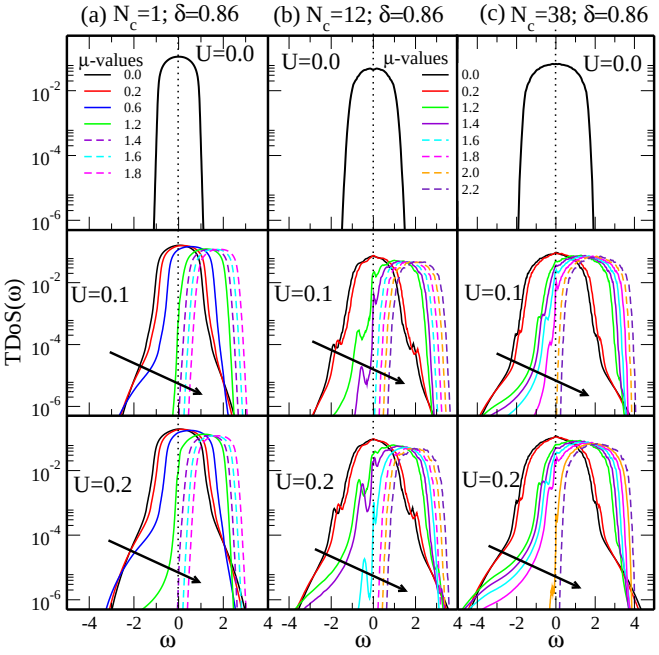

FIG. 3. (Color online). The evolution of the TDoS of the AHM for increasing U-values for the TMT ($N_c = 1$, (**a**)) and finite clusters ($N_c = 12$ (**b**) and 38 (**c**)) at fixed $\delta = W/W_c^U = 0.86$ on a log-linear plot for increasing μ-values. For $U = 0.0$, we show the plot for $\mu = 0$ only, since changing μ only involves a rigid shift of the TDoS. For $U > 0$, notice the systematic disappearance of the exponential tails (indicated by arrow) and the non-trivial decrease of the TDoS for the finite U (unlike the rigid shift in $U = 0$) as one approaches the mobility edge energy.

both constrained by the Pauli principle. I.e., the inelastic scattering vanishes as $\omega \to 0$. However, if we apply the same logic to an interacting disordered system, then, we might expect the edge of the TDoS to be smeared out by these inelastic scattering processes, whenever the edge energy is above the Fermi energy, but become sharp as the edge, approaches it. Though, some argue that this reasoning fails for a disordered system, especially for a strongly disordered system since a well-defined quasiparticle no longer exists [45]. As a consequence, the concept of a mobility edge would not hold and the TDoS should have pronounced exponential "tails" even when the Fermi energy approaches the top or bottom of the TDoS bands. As it is evident from Fig. 3, the sharp mobility edge is restored as the mobility edge energy is approached in tandem with the Fermi liquid description.

The smearing of the TDoS edge can further be inferred from the convolutions found in the second order (and higher) diagrams (cf. Fig. 1), which will mix states above and below the non-interacting localization edge. Consider two such states: one localized and the other extended, which are now degenerate due to this mixing. Since these states hybridize with each other, both states will become extended [6].

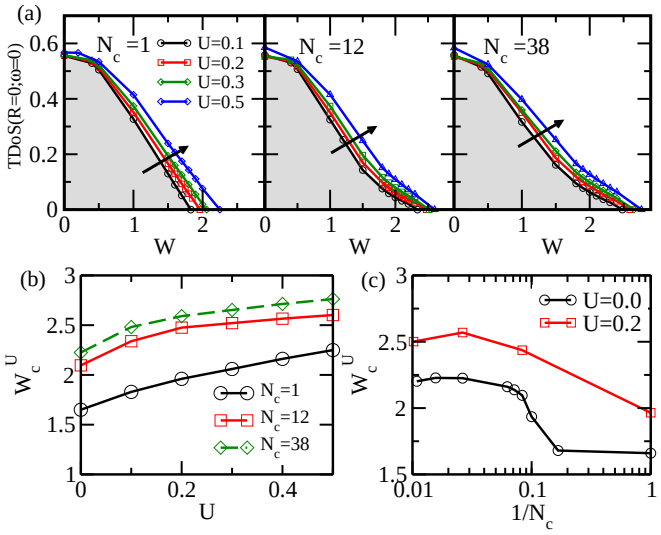

FIG. 4. (Color online). (**a**) The evolution of the TDoS (at $\omega = 0$) as a function of the disorder strength W for various interactions for $N_c = 1$, 12, and 38 at half-filling. The integral $\int \Im\Gamma(K,\omega)\, dK\, d\omega$ vanishes at the same W_c as the TDoS for a given U (not shown), signifying that the absence of the hybridization paths leads to the vanishing of the TDoS. As indicated by the arrow, increasing U pushes W_c to larger values. (**b**) The interaction dependence of the critical disorder W_c^U for different cluster sizes $N_c = 1$, 12, and 38 of the AHM at half-filling. The unit is fixed by setting $4t = 1$. The plot is generally in agreement with the results of Ref. [46]. (**c**) The W_c^U vs $1/N_c$ on a semi-log plot at $U = 0.0$ and $U = 0.2$ for the half-filled AHM. Note the systematic and fast convergence of W_c^U with cluster size for both cases.

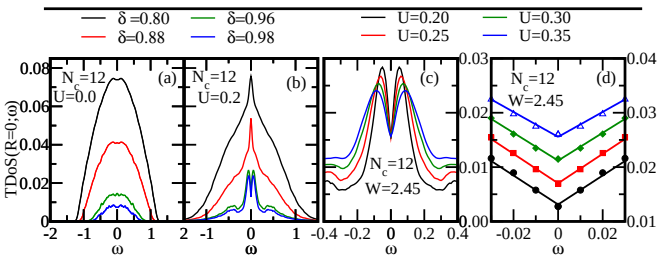

FIG. 5. (Color online). The TDoS vs energy (ω) for $N_c = 12$ ($U = 0.0$) (**a**) and $N_c = 12$ ($U = 0.2$) (**b**) at various $\delta = W/W_c^U$ showing the formation of a pseudogap at intermediate W just before $W_c^{U=0.2}$, which is absent when $U = 0$. (**c**) Shows the TDoS vs ω at a fixed W (close to $W_c^{U=0.2} = 2.50$) for various U. Note, the data has been scaled with U. (**d**) Same data as in Fig. 5(c) showing the linear dependence of the pseudogap on ω.

Next, we explore the effect of interactions on the half-filled, disorder-driven localization transition. We show in Fig. 4 the evolution of the TDoS at the band center, $\omega = 0$, for various cluster sizes. The integrated escape rate ($\int \Im\Gamma(K,\omega) dK d\omega$) (not shown) characterizes the rate of diffusion of electrons between the impurity/cluster and the typical medium. The vanishing of the hybridization paths leads to a localization transition. The TDoS vanishes at the same value of W_c^U as the integrated escape rate.

Figure 4(a) shows that an increase in U from 0.1 to 0.5 leads to a concomitant increase in W_c^U. One can say loosely that, the zero-temperature effect of correlations is an effective reduction in the disorder strength [32, 44], leading to the increase in W_c as indicated by the arrow. For the TMT ($N_c = 1$), the W_c^U increases as 1.83, 1.96, 2.06, 2.22, and 2.25 for $U = 0.1 - 0.5$, while for the TMDCA ($N_c = 12$), W_c^U increases as 2.34, 2.48, 2.52, 2.57, and 2.60, and for for the TMDCA ($N_c = 38$) as 2.48, 2.59, 2.65, 2.71, and 2.76 for $U = 0.1 - 0.5$. We note that W_c^U increases more quickly with U as one goes from single-site ($N_c = 1$) to finite clusters ($N_c = 12$ and 38). This is likely due to the effect of a finite U on the coherent backscattering, which is absent for $N_c = 1$ and is systematically incorporated as N_c increases.

In Figure 4(b), we show the interaction U dependence of the critical disorder strength W_c^U for $N_c = 1$, 12, and 38 for the half-filled AHM. For each of the N_c, we obtain a correlated metal below the lines, and above we have the gapless Anderson-Mott insulator. The trend in both the single site and finite cluster are alike (i.e., W_c^U increases with increasing U) except for the difference in W_c^U. The almost linear trend observed for the low U is in agreement with previous studies [31, 46]. Figure 4(c) depicts the W_c^U as a function of $1/N_c$ at $U = 0.0$ and $U = 0.2$ for the half-filled AHM. Note the systematic and fast convergence of W_c with N_c for both cases.

We further show in Fig. 5 the evolution of the TDoS(ω) for $N_c = 12$ at $U = 0.0$ (Fig. 5(a)) and 0.2 (Fig. 5(b)) for various $\delta = W/W_c^U$. For finite U a soft-pseudogap, which is linear in ω (cf. Fig.5(d)) develops at the Fermi energy (note, this is true irrespective of electron filling) at intermediate disorder strengths immediately before the system becomes localized. In Fig. 5(c), we show that the pseudogap is robust as a function of $U < 1$. Noting that we have only short-range interaction, this soft-pseudogap cannot be attributed to excitonic effects (which are negligible here) as in the Efros-Shklovskii theory [21]. Also, since it occurs only in the TDoS and even for $N_c = 1$, it cannot be due to the multivalley structure of the energy landscape [47] since a single-site cannot generate a multivalley energy landscape to sustain sets of metastable states, and it should be contrasted from the Altshuler-Aronov zero-bias anomaly, which is due to weak nonlocal interactions and weak disorder [48]. We ascribed this soft pseudogap to the same scenario, which causes well-defined mobility edge to only exist when $\mu \gtrsim \omega_\epsilon$. U suppresses localization and increases the TDoS. However, near the Fermi energy the phase space for scattering by U is drastically reduced leading to the opening of a soft pseudogap. Put differently, the pseudogap is due to the suppression of inelastic scattering by U due to the Pauli principle and energy conservation. It is linear (cf.

Fig.5(d)), rather than quadratic in ω, due to the lack of momentum conservation.

Conclusions– Based on experiment, theory, and simulations, there is a growing consensus that the local density of states in a disordered system develops a highly skewed [49], log-normal distribution [9, 29, 50] with a typical value given by the geometric mean that vanishes at the localization transition, and hence, acts as an order parameter for the ALT. New mean field theories for localization, including the TMT and its cluster extension, the TMDCA, have been proposed. In this letter, we extend the TMDCA to weakly interacting systems using second order perturbation theory. We find that weak local interactions lead to an increase in W_c, with the localization edge preserved when the chemical potential is at or above the mobility edge energy. For finite U we observe a soft-pseudogap for values of the disorder strength just above W_c^U.

Acknowledgments– This work is supported by NSF DMR-1237565 and NSF EPSCoR Cooperative Agreement EPS-1003897. Supercomputer support is provided by the Louisiana Optical Network Initiative (LONI) and HPC@LSU.

* Electronic address: cekuma1@lsu.edu
† Electronic address: jarrellphysics@gmail.com

[1] P. W. Anderson, Phys. Rev. **109**, 1492 (1958).
[2] E. Abrahams, P. W. Anderson, D. C. Licciardello, and T. V. Ramakrishnan, Phys. Rev. Lett. **42**, 673 (1979).
[3] F. Wegner, Z. Phys. B **35**, 207 (1979).
[4] B. Kramer and A. MacKinnon, Rep. Prog. Phys. **56**(12), 1469 (1993).
[5] F. Evers and A. D. Mirlin, Rev. Mod. Phys. **80**, 1355 (2008).
[6] N. Mott, Adv. Phys. **16**(61), 49 (1967); *ibid.* Proc. Phys. Soc., Sect. A **62**, 416 (1949); *ibid. Metal-Insulator Transitions, 2nd ed.* (Taylor and Francis, London, 1990).
[7] E. Abrahams (ed.) *50 Years of Anderson Localization* (World Scientific, 2010).
[8] D. Belitz and T. R. Kirkpatrick, Rev. Mod. Phys. **66**, 261 (1994).
[9] A. Richardella, P. Roushan, S. Mack, B. Zhou, D. A. Huse, D. D. Awschalom, and A. Yazdani, science **327**, 665 (2010).
[10] S. V. Kravchenko, G. V. Kravchenko, J. E. Furneaux, V. M. Pudalov, and M. D'Iorio, Phys. Rev. B **50**, 8039–8042 (1994).
[11] K. Maiti, R. S. Singh, and V. R. R. Medicherla, Phys. Rev. B **76**, 165128 (2007).
[12] K. W. Kim, J. S. Lee, T. W. Noh, S. R. Lee, and K. Char, Phys. Rev. B **71**, 125104 (2005).
[13] R. K. Sahu, S. K. Pandey, and L. Pathak, J. Solid State Chem. **184**(3), 523 – 530 (2011).
[14] A. S. Sefat, J. E. Greedan, G. M. Luke, M. Niéwczas, J. D. Garrett, H. Dabkowska, and A. Dabkowski, Phys. Rev. B **74**, 104419 (2006).
[15] A. Raychaudhuri, Adv. Phys. **44**(1), 21 (1995).
[16] L. Sanchez-Palencia and M. Lewenstein, Nature Physics **6**(2), 87 (2010).
[17] B. Shapiro, J. Phys. A: Math. and Theor. **45**(14), 143001 (2012).
[18] M. White, M. Pasienski, D. McKay, S. Q. Zhou, D. Ceperley, and B. DeMarco, Phys. Rev. Lett. **102**, 055301 (2009).
[19] S. S. Kondov, W. R. McGehee, W. Xu, and B. DeMarco, Phys. Rev. Lett. **114**, 083002 (2015).
[20] B. L. Altshuler and A. G. Aronov, JETP Lett. **27**, 662 (1978).
[21] A. L. Efros and B. I. Shklovskii, J. Phys. C: Solid State Physics **8**(4), L49 (1975).
[22] A. Finkel'stein, JETP **57**, 97 (1983).
[23] C. Castellani, C. Di Castro, P. A. Lee, and M. Ma, Phys. Rev. B **30**, 527–543 (1984).
[24] A. Punnoose and A. M. Finkel'stein, Science **310**(5746), 289 (2005).
[25] S. Anissimova, S. V. Kravchenko, A. Punnoose, A. M. Finkel/'stein, and T. M. Klapwijk, Nat Phys **3**(10), 707–710, ISSN 1745-2473 (2007).
[26] C. E. Ekuma, H. Terletska, K.-M. Tam, Z.-Y. Meng, J. Moreno, and M. Jarrell, Phys. Rev. B **89**, 081107 (2014).
[27] V. Dobrosavljević, A. A. Pastor, and B. K. Nikolić, EPL **62**(1), 76 (2003).
[28] G. Schubert, J. Schleede, K. Byczuk, H. Fehske, and D. Vollhardt. Phys. Rev. B **81**, 155106 (2010).
[29] W. Li, X. Chen, L. Wang, Y. He, Z. Wu, Y. Cai, M. Zhang, Y. Wang, Y. Han, R. W. Lortz, Z.-Q. Zhang, P. Sheng, and N. Wang, Sci. Rep. **3**, 1772 (2013).
[30] M. C. O. Aguiar and V. Dobrosavljević, Phys. Rev. Lett. **110**, 066401 (2013).
[31] M. C. O. Aguiar, V. Dobrosavljević, E. Abrahams, and G. Kotliar, Phys. Rev. Lett. **102**, 156402 (2009).
[32] K. Byczuk, W. Hofstetter, and D. Vollhardt, Int. J. Mod. Phys. B **24**, 1727 (2010).
[33] A. N. Rubtsov, V. V. Savkin, and A. I. Lichtenstein, Phys. Rev. B **72**, 035122 (2005).
[34] A. N. Rubtsov and A. I. Lichtenstein, JETP Lett. **80**, 61 (2004).
[35] E. Gull, A. J. Millis, A. I. Lichtenstein, A. N. Rubtsov, M. Troyer, and P. Werner, Rev. Mod. Phys. **83**, 349 (2011).
[36] E. Gull, P. Werner, O. Parcollet, and M. Troyer, EPL **82**(5), 57003 (2008).
[37] S. Fuchs, E. Gull, M. Troyer, M. Jarrell, and T. Pruschke, Phys. Rev. B **83**, 235113 (2011).
[38] J. E. Hirsch and R. M. Fye, Phys. Rev. Lett. **56**, 2521–2524 (1986).
[39] N. Blümer, Phys. Rev. B **76**, 205120 (2007).
[40] F. Gebhard, E. Jeckelmann, S. Mahlert, S. Nishimoto, and R. Noack, Euro. Phys. B **36**(4), 491–509 (2003).
[41] M. Frigo and S. Johnson. "FFTW: An adaptive software architecture for the FFT," In *Proc. IEEE Int'l Conf. Acoustics, Speech, and Signal Processing*, vol. 3, Seattle, WA, 1381, (1998).
[42] See Supplemental Material at [URL will be inserted by publisher] for the benchmarking of our developed TMDCA-SOPT with quantum Monte-Carlo simulations both for single-site ($N_c = 1$) and finite cluster ($N_c = 14$) for the Anderson-Hubbard model. As it is evident from the comparisons, the agreement in the parameter regime we explored is remarkable even up to relatively large

value of U. This good agreement not only validates our assumption that higher order diagrams are suppressed by at least $\sim (U^3)$, but provides a comprehensive benchmark of the capabilities of the developed finite cluster formalism.

[43] M. Ma, Phys. Rev. B **26**, 5097 (1982).

[44] D. Tanasković, V. Dobrosavljević, E. Abrahams, and G. Kotliar, Phys. Rev. Lett. **91**, 066603 (2003).

[45] D. Golubev and A. Zaikin. Physica B **255**, 164 (1998); *ibid.* D. S. Golubev, C. P. Herrero, and A. D. Zaikin. EPL **63**, 426 (2003).

[46] K. Byczuk, W. Hofstetter, and D. Vollhardt, Phys. Rev. Lett. **94**, 056404 (2005).

[47] H. Shinaoka1 and M. Imada, J. Phys. Soc. Jpn. **78**, 094708 (2009).

[48] B. L. Altshuler and A. G. Aronov, Sov. Phys. JETP **50**, 968 (1979); *ibid.* Solid State Communs. **30**, 115 (1979).

[49] R. Sapienza, P. Bondareff, R. Pierrat, B. Habert, R. Carminati, and N. F. van Hulst, Phys. Rev. Lett. **106**, 163902 (2011).

[50] I. S. Burmistrov, I. V. Gornyi, and A. D. Mirlin, Phys. Rev. Lett. **111**, 066601 (2013).